doi:10.1246/cl.2012.552
Published on the web April 28, 2012

# One-step Fabrication of Polystyrene–$TiO_2$ Nanosandwich Film by Phase Separation

Naoki Mizutani,[1] Sergiy Korposh,[1] Roman Selyanchyn,[1] Do-Hyeon Yang,[1]
Chang-Soo Lee,[3] Seung-Woo Lee,*[1] and Toyoki Kunitake[2]
[1]*Graduate School of Environmental Engineering, The University of Kitakyushu, 1-1 Hibikino, Kitakyushu, Fukuoka 808-0135*
[2]*Kitakyushu Foundation for the Advancement of Industry, Science and Technology, 2-1 Hibikino, Kitakyushu, Fukuoka 808-0135*
[3]*Bionanotechnology Research Center, Korea Research Institute of Bioscience and Biotechnology, 111 Gwahangno, Yuseong-gu, Daejeon 305-806, Korea*

(Received February 8, 2012; CL-120104; E-mail: leesw@kitakyu-u.ac.jp)

A polystyrene–$TiO_2$ nanosandwich film was fabricated by spin-coating a mixture of PS and Ti(O-*n*-Bu)$_4$. Phase separation of the two components showed various morphological changes in the film, depending on the PS concentration, and sandwich-like phase separation was achieved for the first time. Doping pyrene as a fluorescent probe was employed to confirm the configuration of PS inside the nanosandwich structure.

Polymer films are widely used for practical applications such as protection, reflection, transistors, hydrofuge, photolithography, and optical displays.[1–3] Smooth, unstructured polymer films can be prepared by spinning a polymer solution. However, when a mixture of different polymers is used, the polymers may be phase-separated and form many unique morphologies.[4] Especially in cases of semiconducting polymers for photodiodes and photovoltaic devices, phase-separated microstructures play highly important roles for the localization and separation of excitons in the interface.[5–7] The phase separation of polymers is also applied to the designed fabrication of various nanostructures. Recently, Shimomura et al. reported a facile fabrication process of polymer particles with controlled sizes and internal structures and named it self-organized precipitation (SORP) method.[8]

The chemical and physical properties of polymer films can be drastically improved through hybridization with inorganic materials,[9,10] in which functionality and flexibility of organic moieties can be combined with robustness and stability of the inorganic part. For instance, uniform, robust hybrid nanomembranes that have nanometer thickness and extremely high aspect ratio (size/thickness) could be fabricated by taking advantage of the interpenetrating network (IPN) between the sol–gel inorganic matrix and the crosslinked polyacrylate polymer.[11] The major purpose of this study is to explore phase separation of spin-coated films made of metal alkoxide and polymer, e.g., Ti(O-*n*-Bu)$_4$ and polystyrene (PS), in order to fabricate nanofilm having a unique structure.

PS-anchored $TiO_2$ hybrid ($PS_x$@$TiO_2$) nanofilms, where $x$ means the mole percent (mol %) of the styrene monomer unit relative to that of Ti(O-*n*-Bu)$_4$, were fabricated as follows: At first, 163 mg of PS was dissolved in 5 mL of chloroform, to give a concentration of 3.26 wt % (1000 μmol). Then, the PS solution was mixed with Ti(O-*n*-Bu)$_4$ (1000 μmol in 5 mL of chloroform) and additional chloroform to achieve an appropriate ratio of Ti(O-*n*-Bu)$_4$ and PS (Table S1).[17] The film forming solutions (400 μL) were spin-coated on a cleaned silicon wafer at a speed of 3000 rpm for 2 min under nitrogen atmosphere.

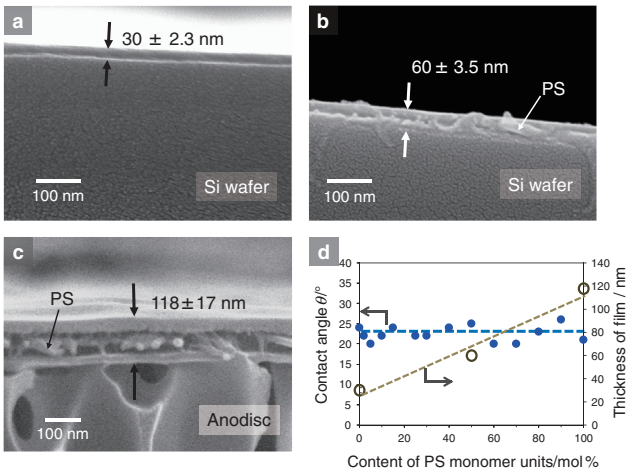


**Figure 1.** Cross-sectional SEM images of (a) pure $TiO_2$, (b) $PS_{50}$@$TiO_2$, and (c) $PS_{100}$@$TiO_2$ nanofilms. (d) Dependence of surface contact angle and thickness on PS content.

Cross-sectional SEM measurements of the $PS_x$@$TiO_2$ nanofilms on the silicon substrate allowed elucidation of how the $TiO_2$ gel and PS components exist inside the film. The thickness of $PS_x$@$TiO_2$ nanofilms depends on the concentration of PS, as compared in Figure 1, and is changed in the range of 30–120 nm under the given preparation conditions (Figure 1d).

Interestingly, the $PS_x$@$TiO_2$ films at $x \geq 50$ are vertically phase-separated, showing a sandwich-like film structure that has two flat layers on the top and at the bottom, as can be seen in the $PS_{100}$@$TiO_2$ film (Figure 1c). This three-layered nanosandwich structure is more pronounced at higher PS concentrations, and the thickness of the middle layer increases when the PS concentration increases. The middle layer of the film is elongated, when the film is vertically cut for the SEM measurement, indicating that the middle layer is flexible PS polymer.

The suface morphology of the prepared films has significantly changed with the increase in the PS concentration, as can be seen from the atomic force microscopic (AFM) images of Figures 2b–2f. The $PS_5$@$TiO_2$ film revealed a surface covered with particles (nanodots) 30–100 nm in diameter and 30–40 nm in height (Figure S1b).[17] With further increase in the PS concentration, the nanodots become networked at $x = 15$ ($PS_{15}$) and aggregated to flat areas at $x = 30$ ($PS_{30}$). The nanodot structure observed at lower concentrations of PS completely disappeared in the $PS_{50}$@$TiO_2$ and $PS_{100}$@$TiO_2$ films to give uniform surfaces.

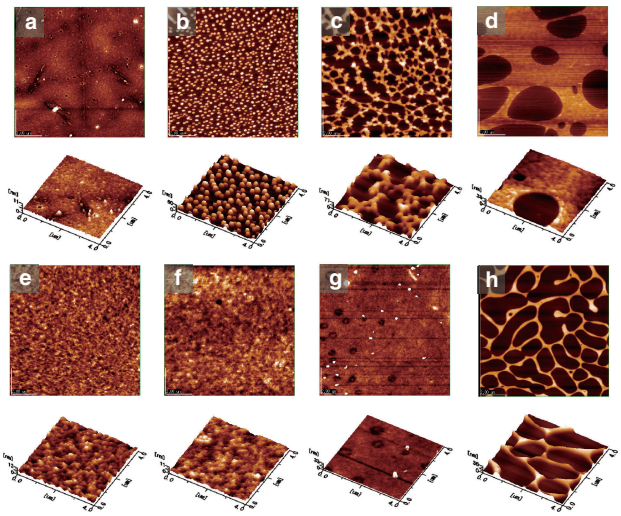


**Figure 2.** AFM images (10 μm × 10 μm, top) and their 3D images (4 μm × 4 μm, bottom) of $PS_x$@$TiO_2$ nanofilms: (a) pure $TiO_2$, (b) $PS_5$@$TiO_2$, (c) $PS_{15}$@$TiO_2$, (d) $PS_{30}$@$TiO_2$, (e) $PS_{50}$@$TiO_2$, (f) $PS_{100}$@$TiO_2$, (g) pure PS, and (h) toluene-based $PS_{25}$@$TiO_2$.

On the other hand, as shown in Figure 2h, when toluene was used as solvent in place of $CHCl_3$, honeycomb-like phase-separated structure was obtained, indicating that $PS_x$@$TiO_2$ morphologies are strongly dependent on the solvent used.

To confirm the formation process of the nanosandwich structure, UV–vis spectral measurements were carried out with the same films prepared on quartz substrates (Figure S2).[17] Linear increase of the absorbance at 204 nm was observed, which may be assigned to the phenyl ring moiety of PS. However, the absorbance of $TiO_2$ gel at 260 nm gradually increases in the range from $x = 0$ to $x = 15$ ($PS_0$–$PS_{30}$) and reaches saturation in the range from $x = 30$ to $x = 100$ ($PS_{30}$–$PS_{100}$). It appears that $PS_{30}$ becomes a turning point of the morphology changes, at which the absorbance of $TiO_2$ gel increases by ca. 1.5 times compared with that of the pure $TiO_2$ film. Interestingly, the contact angle of the $PS_x$@$TiO_2$ nanofilms showed similar values of ca. 26° for all films, regardless of the PS content (Figure 1d), revealing that the outermost layer of the films is covered with a $TiO_2$ gel layer. The surface morphology of the outermost $TiO_2$ layer in the $PS_{50}$ or $PS_{100}$@$TiO_2$ nanofilms, however, appears to reflect the phase-separated PS structures and is more rugged than that of the pure $TiO_2$ or pure PS film (Figures 2e and 2f).

The nanosandwich ($PS_{100}$@$TiO_2$) film was also studied by reflection interference spectroscopy analysis, which is based on the interference of white light at thin films. For the $PS_{100}$@$TiO_2$ film, the reflection color is blue (Figure 3a), while that of the pure PS film is golden (Figure 3b). This difference in the reflected colors between the pure PS and $PS_{100}$@$TiO_2$ films indicates that they have different film densities and refractive indexes. Using eq 1, the refractive index ($n_f$) of the $PS_{100}$@$TiO_2$ film can be determined with its geometric film thickness obtained by SEM measurement:

$$n_f = \frac{m\lambda_{max}}{2d} \quad (1)$$

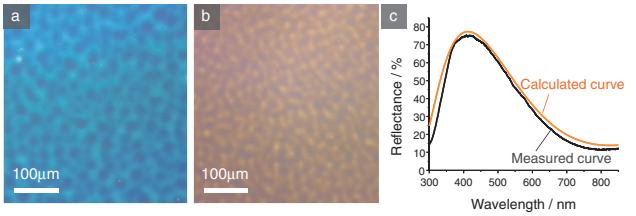


**Figure 3.** Reflection images of (a) $PS_{100}$@$TiO_2$ and (b) pure PS films. (c) Comparision of measured and simulated reflection spectra of the $PS_{100}$@$TiO_2$ nanosandwich film: the simulated curve was obtained using eq 2.

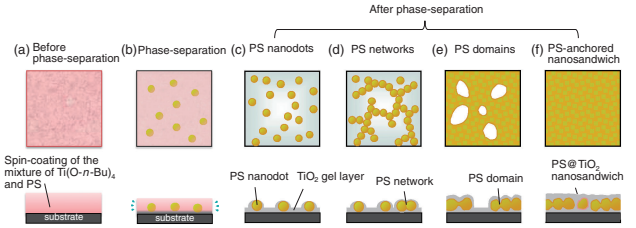


**Figure 4.** Schematic illustration of the surface and cross-section of $PS_x$@$TiO_2$ nanofilms (a) before phase separation, (b) in the beginning of phase separation, and after phase separation: (c) $PS_5$@$TiO_2$, (d) $PS_{15}$@$TiO_2$, (e) $PS_{30}$@$TiO_2$, and (f) $PS_{50–200}$@$TiO_2$, respectively.

where, $m$ is the number of inference fringes; $\lambda_{max}$ is the wavelength at which maximum of the fringe is observed; $n_f$ is the refractive index of the film.

In order to check the feasibility of the proposed calculation using the reflectometric interference spectroscopy, the obtained reflection spectrum was simulated using eq 2:[12]

$$R = \frac{(r_{12} + r_{23})^2 - 4 \cdot r_{12} \cdot r_{23} \cdot \sin\delta}{(1 + r_{12} \cdot r_{23})^2 - 4 \cdot r_{12} \cdot r_{23} \cdot \sin\delta};$$
$$r_{12} = \frac{1 - n_f}{1 + n_f};\ r_{23} = \frac{n_f - n_s}{n_f + n_s};\ \delta = \frac{2 \cdot \pi \cdot n_f \cdot d}{\lambda} \quad (2)$$

where $r_{12}$ and $r_{23}$ are the reflection coefficients from air–film and film–substrate interfaces, respectively; $n_f$ is the refractive index of the film; $n_s$ is the refractive index of the silicon substrate; $d$ is the film thickness. The thickness value of 118 nm obtained from the SEM observation for the $PS_{100}$@$TiO_2$ nanohybrid film was used for simulation. As can be seen from Figure 3c, the simulated spectrum is consistent with the experimentally measured result, when a value of refractive index of 1.75 was used. This means that the refractive index of the $PS_{100}$@$TiO_2$ film may be approximately 1.75 in the middle of those of amorphous $TiO_2$ and PS (2.00[13] and 1.57,[14] respectively).

From these results we propose the formation process of the nanosandwich film, as shown in Figure 4. First, a mixture of Ti(O-*n*-Bu)$_4$ and PS is uniformly deposited on the substrate by spin-coating, and Ti(O-*n*-Bu)$_4$ forms a precursor layer on the hydrophilic surface of the substrate. Then, the condensed PS is transformed into nanodots on the precursor layer, which are then networked and densely aggregated with the increase of the PS concentration. The remaining free Ti(O-*n*-Bu)$_4$ floats on the PS layer and forms an additional layer. The Ti(O-*n*-Bu)$_4$ layer is hydrolyzed by moisture in the atmosphere and turns into a $TiO_2$

  

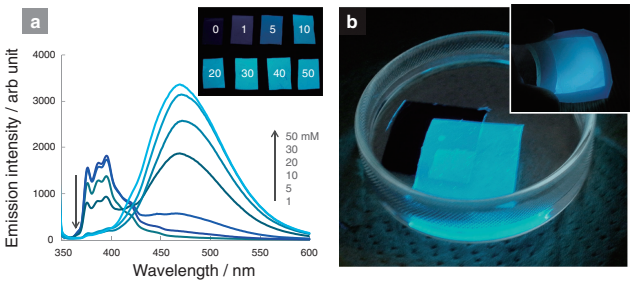


**Figure 5.** (a) Fluorescence spectra of pyrene-doped $PS_{100}@TiO_2$ films with the increase of the pyrene content: the inset shows fluorescence images of the films with different pyrene concentrations. (b) Optical image of a fluorescent free-standing membrane floating on water (30 mM pyrene-doped $PS_{100}@TiO_2$ film): inset shows a photograph of the membrane transferred onto a flexible silicon rubber.

layer. Consequently, the PS–$TiO_2$ nanosandwich film is obtained. It is important to note that the same sandwich structure is not obtainable, when Ti(O-*n*-Bu)$_4$ and PS solutions were alternately spin-coated (data not shown).

An advantage of the phase-separated nanosandwich structures lies in the independent use of the physical and chemical properties of each film component. In this study, we tested incorporation of hydrophobic molecules to the PS layer of the $PS_{100}@TiO_2$ nanosandwich film. Thus, pyrene was added to the Ti(O-*n*-Bu)$_4$/PS precursor solution for $PS_{100}@TiO_2$ film at 0–50 mM. Pyrene-doped $PS_{100}@TiO_2$ films were fabricated by spin-coating. When the prepared films were irradiated by 254 nm UV light, representative fluorescent peaks of pyrene at 395 (monomer) and 470 nm (excimer) were observed and their relative emission intensity was changed with the concentration increase of pyrene, as shown in Figure 5a. The excimer peak reaches saturation at about 30 mM of pyrene. The fluorescence of pyrene is usually quenched in $TiO_2$ matrices (data not shown). Based on these results, we can conclude that pyrene is selectively introduced into the hydrophobic phase of the $PS_{100}@TiO_2$ nanofilm. The observation of fluorescent nanodots also encloses this conclusion (Figure S3).[17]

The free standing property of the PS@$TiO_2$ nanosandwich film is an advantageous feature (details are shown in Figure S4a).[17] Figure 5b shows an optical image of the pyrene (30 mM)-doped free-standing $PS_{100}@TiO_2$ nanomembrane that is floating on the surface of water, which could be even transferred onto a flexible silicon rubber (see inset of Figure 5b).

In conclusion, the current study demonstrates a novel process for creation of specific organic/inorganic hybrid structures in nanofilms. The combination of PS and Ti(O-*n*-Bu)$_4$ provided unique phase-separated nanostructures. The obtained high fluorescence efficiency of the pyrene excimer in the nanohybrid films offers the possibility for new sensor applications.[15,16] We expect that the current approach would provide a new direction of synthesis of hybrid nanomaterials for diverse applications.

This work was supported by the MEXT via the Kitakyushu Knowledge-based Cluster Project and partly by the Fundamental R&D Program for Core Technology of Materials funded by the Ministry of Knowledge Economy, Republic of Korea (grant no: TGC 0300811).

## References and Notes

1 G. ten Brinke, D. Ausserre, G. Hadsiioannou, *J. Chem. Phys.* **1988**, *89*, 4374.
2 T. Matsunobe, N. Nagai, R. Kamoto, Y. Nakagawa, H. Ishida, *J. Photopolym. Sci. Technol.* **1995**, *8*, 263.
3 T. Liang, Y. Makita, S. Kimura, *Polymer* **2001**, *42*, 4867.
4 S. Y. Heriot, R. A. L. Jones, *Nat. Mater.* **2005**, *4*, 782.
5 J. J. M. Halls, A. C. Arias, J. D. MacKenzie, W. Wu, M. Inbasekaran, E. P. Woo, R. H. Friend, *Adv. Mater.* **2000**, *12*, 498.
6 D. C. Coffey, D. S. Ginger, *Nat. Mater.* **2006**, *5*, 735.
7 A. C. Morteani, A. S. Dhoot, J.-S. Kim, C. Silva, N. C. Greenham, C. Murphy, E. Moons, S. Ciná, J. H. Burroughes, R. H. Friend, *Adv. Mater.* **2003**, *15*, 1708.
8 H. Yabu, T. Higuchi, K. Ijiro, M. Shimomura, *Colloids Surf., A* **2006**, *250*, 284.
9 R. Tamaki, Y. Chujo, *Chem. Mater.* **1999**, *11*, 1719.
10 D. Kessler, P. Theato, *Macromolecules* **2008**, *41*, 5237.
11 R. Vendamme, S.-Y. Onoue, A. Nakao, T. Kunitake, *Nat. Mater.* **2006**, *5*, 494.
12 P. D. T. Huibers, D. O. Shah, *Langmuir* **1997**, *13*, 5995.
13 T. Sasaki, Y. Ebina, T. Tanaka, M. Harada, M. Watanabe, G. Decher, *Chem. Mater.* **2001**, *13*, 4661.
14 L. H. Garcia-Rubio, *Macromolecules* **1992**, *25*, 2608.
15 K. Kokado, T. Iwamura, Y. Chujo, *Polym. J.* **2008**, *40*, 402.
16 H. Yoshida, H. Harada, Y. Nakano, H. Nohta, J. Ishida, M. Yamaguchi, *Biomed. Chromatogr.* **2004**, *18*, 687.
17 Supporting Information is available electronically on the CSJ-Journal Web site, http://www.csj.jp/journals/chem-lett/index.html.

  